ACS APPLIED MATERIALS & INTERFACES

RESEARCH ARTICLE

www.acsami.org

Effect of Fullerene Intercalation on the Conformation and Packing of Poly-(2-methoxy-5-(3′-7′-dimethyloctyloxy)-1,4-phenylenevinylene)

Adam J. Wise, Mimi R. Precit, Alexandra M. Papp, and John K. Grey*

Department of Chemistry and Chemical Biology, MSC03 2060, University of New Mexico, Albuquerque, New Mexico 87131, United States

Supporting Information

ABSTRACT: Photoluminescence (PL) and resonance Raman spectroscopy are used to track changes in the conformations and packing of poly-(2-methoxy-5-(3′-7′-dimethyloctyloxy)-1,4-phenylenevinylene) (MDMO-PPV) chains with the addition of [6,6]-phenyl-C_{61}-butyric acid methyl ester (PCBM) molecules. PL lineshapes of MDMO-PPV thin films as a function of annealing time were first measured to determine the spectroscopic signatures of chain conformations and packing in the absence of PCBM. Annealing results in enhanced interchain interactions leading to red-shifts of PL 0−0 transitions by up to ∼300 cm^{-1} and apparent increases of the line shape Huang−Rhys factors. Wavelength-dependent PL lifetimes of as-cast and films annealed for short times (∼30 s) are nonexponential with an instrument-limited component of ∼100 ps and a ∼350 ps component. With longer annealing times, decays become single exponential with an average lifetime of ∼1 ns indicating that all excitations efficiently funnel to strongly coupled interchain sites. Addition of PCBM disrupts MDMO-PPV interchain interactions causing PL 0−0 transitions to blue-shift, increases in line width, and decreases in apparent Huang−Rhys factors. Resonance Raman spectra of MDMO-PPV/PCBM thin films with variable PCBM weight fractions (∼50:1 up to 1:8 w/w) were then measured using short (488 nm) and long (568 nm) excitation wavelengths. The out-of-plane vinylene C−H wag mode of MDMO-PPV (∼964 cm^{-1}) showed pronounced increases in intensity of up to ∼30% and red-shifts of up to 5 cm^{-1} with increasing PCBM content. These changes result from a decrease of planarity between chain segments that suppresses interchain interactions. Furthermore, red-shifts of up to ∼4 cm^{-1} were observed for the C═C symmetric stretch of the MDMO-PPV vinylene group (∼1625 cm^{-1}) with 488 nm excitation. The sensitivity of the MDMO-PPV vinylene group vibrations with PCBM indicates preferential interactions between these two molecules and is consistent with intercalation of PCBM into the polymer structure. This assignment was confirmed by thermally annealing of MDMO-PPV/PCBM films to remove intercalated PCBM molecules, which partially restores interchain interactions as seen from smaller intensity increases (∼15%) and red-shifts (∼2 cm^{-1}) of the ∼964 cm^{-1} mode. Overall, the spectroscopic results show that MDMO-PPV chains adopt distorted conformations (i.e., less intrachain order and shorter conjugation lengths) that have important implications for explaining the structural origins for large improvements in charge mobilities in MDMO-PPV/PCBM blends.

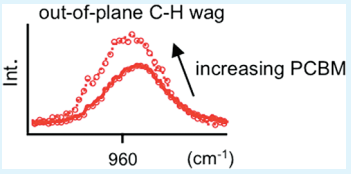

KEYWORDS: conjugated polymers, intercalation, planarity, resonance Raman spectroscopy

INTRODUCTION

The conformational and packing characteristics of conjugated polymer chains in polymer/fullerene solar cell blends plays a vital role in determining overall material performance.[1−4] Recent structural studies have shed light on the nature of interaction between polymers and fullerene additives,[5,6] and new insights into the structural factors influencing optimal polymer/fullerene loadings and morphology are beginning to emerge.[7−10] For example, the miscibility of polymer and fullerene component plays a significant role in determining film morphology, which depends on molecular-level structure and interactions. It was recently proposed that when there is sufficient volume between solubilizing side groups (>1 nm) the fullerene molecules can intercalate into the polymer structure leading to an intimately mixed phase.[5,6,11] The most compelling evidence for this effect was shown recently for X-ray studies of poly-(2,5-bis(3-tetradecyllthiophen-2-yl)thieno[3,2-b]thiophene) (PBTTT) where interchain spacing increased upon addition of a fullerene derivative.[5] This feature also explains why nonintercalating polymers (i.e., poly-3-hexylthiophene) exhibit optimal polymer/fullerene loading ratios of ∼1:1 w/w, whereas intercalating systems show optimal loadings as high as 1:4 w/w, such as PBTTT.

Unfortunately, not all structural studies of polymers can employ X-ray techniques due to the lack of extended order (crystallinity) and intercalation must be inferred indirectly from optimal loading characteristics used in solar cell devices, changes in charge mobilities and PL quenching. One such example is the well-studied poly-[2-methoxy-5-[3′,7′-dimethyloctyloxy)-1,4-phenylenevinylene] (MDMO-PPV) system that requires high fullerene loadings (1:4 w/w) to achieve reasonable solar cell power conversion efficiencies (∼3%). Interestingly, charge (hole) mobility measurements of MDMO-PPV/fullerene thin films (1:4 w/w) showed large increases (about 2 orders of magnitude) compared to pristine MDMO-PPV films.[12,13] The

Received: April 25, 2011
Accepted: July 7, 2011
Published: July 07, 2011

longstanding explanation for these increases is that MDMO-PPV chains uncoil and elongate with the addition of PCBM resulting in higher intrachain order (i.e., increased conjugation length and planarity between segments) and increased interchain interactions.[12,13] More recently, McGehee and co-workers proposed that intercalation of acceptor molecules is responsible for enhancement of charge mobility in MDMO-PPV blends, which was inferred from space-charge limited current (SCLC), PL quenching, and electron microscopy studies of various MDMO-PPV/acceptor blends.[11] Only proposed intercalating acceptors (i.e., fullerenes) showed increased hole mobilities whereas other small molecules had little effect on measured charge mobilities.[11] When MDMO-PPV/fullerene blend films are annealed, phase separation occurs and SCLC mobility values return to approximately the original pristine polymer values.[11] Because of the inability of PL quenching and X-ray techniques to directly report on the polymer structure chain conformation and packing changes in MDMO-PPV blends, it is necessary to seek alternative methods to fully understand the role of fullerene intercalation on polymer conformations and packing.

Raman spectroscopy is such a technique that, with its high sensitivity and selectivity, can unravel the structural attributes of polymer chains in blend films. Raman spectroscopy is based on a two-photon inelastic scattering process and allows for sensitive and nondestructive investigations of chemical structure and changes with material processing conditions. By careful choice of excitation wavelengths, it is possible to selectively interrogate a single component in complex systems by tuning the laser to a particular optical transition. This resonance excitation scheme typically results in large enhancements of Raman scattering cross-sections for certain vibrational modes (i.e., Franck−Condon active modes) that also greatly simplify the Raman spectrum.[14] Resonance Raman spectroscopy is especially useful for investigating polymer/fullerene blends since polymer PL backgrounds are strongly suppressed. This feature makes Raman transitions easily discernible that are normally overwhelmed by background shot noise. Furthermore, polymer backbone vibrations are highly sensitive to minor changes in the local environment and the presence of dopants. This feature makes Raman spectroscopy an excellent tool for understanding chain conformation and packing effects on electronic properties such as conjugation lengths and polaron formation.[15−17] Furthermore, Raman techniques are amenable to mapping studies that can reveal the spatial variation of chemical structure and packing on submicrometer size scales.[2,18,19] Resonance Raman spectroscopy has also seen use in characterizing the structural attributes of donor/acceptor charge transfer complexes that have recently been applied to polymer/acceptor systems.[20,21]

Because of the complexity of donor/acceptor polymer blends, it is first necessary to understand spectroscopic reporters of polymer chain conformational and packing characteristics in the absence of acceptors. For example, there has been a great deal of interest and controversy surrounding the existence and physical origin of so-called aggregate or interchain excitons in related PPV systems.[22−25] The relative amounts of these species as well as interchain electronic coupling strength can also be modified by the addition of acceptors (i.e., fullerenes), which makes the understanding of chain packing and order crucial for the continued optimization of polymer solar cell performance. Aggregate species have been studied extensively using frequency- and time-resolved spectroscopy as well as scanned probe techniques. The general consensus from this body of work is that slow solvent evaporation and/or annealing of films leads to a greater number of interchain aggregate species.[1] However, Janssen and co-workers showed that MDMO-PPV chains tend to self-aggregate and adopt coiled conformations due to the asymmetric backbone substitution pattern and do not change upon annealing.[26,27] Regardless of the type of aggregate, both inter- and intrachain aggregates show similar red-shifted PL maxima, diminished yields, and sometimes non-Poissonian lineshapes.[28,29] Application of hydrostatic pressures have demonstrated similar trends in PL spectra where pressure causes polymer chain segments to planarize and close-pack thus forming more aggregate sites.[30]

Although shifting PL energies and changes in PL lifetimes are effective diagnostics of the chain packing characteristics, the vibronic line shape parameters (i.e., Huang−Rhys factors and linewidths) also provide valuable insight into the polymer structure and changes in molecular geometry between ground and excited states. We recently showed that the experimental vibronic intervals in MDMO-PPV PL spectra do not match any ground state vibrational frequency which is known as the missing mode effect (MIME).[31] The MIME arises from the coalescence of transitions from several displaced modes that results in an effective PL vibronic interval and the values of the MIME intervals are determined by the relative displacement (Huang−Rhys factor) of each Franck−Condon active mode as well as its frequency.[32] Importantly, the contribution of each mode to the observed MIME interval in polymer PL spectra can be affected by changes in conformational and packing that are affected by material processing conditions. Despite the usefulness of PL line shape analysis for understanding processing-dependent variations in vibrational displacements and polymer structure, this approach can be rather limited when applied to polymer/acceptor blends owing to strong PL quenching, overlapping transitions and increased line width broadening typically encountered in samples with large acceptor loadings.

Here we use a combination of resonance Raman and PL spectroscopy to investigate the effect of MDMO-PPV structure upon addition of the soluble fullerene derivative, [6,6]-phenyl-C_{61}-butyric acid methyl ester (PCBM). Chain conformation and packing interactions and their impact on excited state relaxation to low energy interchain sites are first studied in the absence of PCBM to identify and understand the spectroscopic markers of conformational and packing arrangements of these molecules. Both frequency- and time-resolved PL spectra reveal changes in line shape, energy, and dynamics upon thermal annealing that are indicative of increased interchain site formation. Addition of PCBM inhibits interchain interactions and PL lineshapes bear increasing resemblance to those of dilute solution samples, i.e., blue-shifted 0−0 transition energies and lower apparent Huang−Rhys factors. However, the strong quenching of MDMO-PPV PL with high PCBM loadings (>1:1 w/w) makes the use of PL spectroscopy difficult to reliably understand chain conformation and packing characteristics from lineshapes alone. Resonance Raman spectroscopy is then used to selectively study MDMO-PPV conformational and packing characteristics with various PCBM loadings (~50:1 up to 1:8 w/w, MDMO-PPV/PCBM). Short (488 nm) and long (568 nm) excitation wavelengths are employed to excite high and low energy regions of MDMO-PPV optical absorption transitions, respectively, that reveals insights into the nature of MDMO-PPV/PCBM interactions for short and long chain segments. As PCBM content increases, the out-of-plane vinylene C−H band of MDMO-PPV

(~964 cm^{-1}) showed substantial increases in intensity and line width as well as red-shifts for both excitation wavelengths. These trends indicate decreasing intrachain order, namely, a loss of coplanarity between polymer chain segments and lower conjugation lengths. These distortions are consistent with the observed blue-shifting of PL energies measured from blends. The C=C symmetric stretching mode of the MDMO-PPV vinylene group (~1625 cm^{-1}) also shows similar intensity increases and red-shifts for 488 nm excitation only that, together with the shifts of the out-of-plane C−H vinylene wag, demonstrates that PCBM interacts preferentially with this backbone group.

We propose that the high sensitivity of the vinylene group vibrations is consistent with intercalation of PCBM molecules into the polymer side groups. However, the PCBM-induced deformations of the MDMO-PPV structure determined from Raman data are not consistent with the previously proposed structural origins for charge mobility enhancements in these blends.

EXPERIMENTAL SECTION

MDMO-PPV (M_n = 26 kDa, PDI = 3.3) and PCBM (ADS) were purified by methanol extraction from chloroform. The remaining fractions were dried and dissolved separately in anhydrous chlorobenzene (Sigma Aldrich) at a concentration of 5 mg/mL and stirred for 24 h inside a nitrogen atmosphere in a glovebox. The solutions were filtered through 200 nm PTFE syringe filters (Whatman) to remove any remaining solids. MDMO-PPV was blended with PCBM in solution in varying weight fractions (i.e., 50:1 up to 1:8 w/w, MDMO-PPV/PCBM) and thin films were prepared by spin-casting solutions onto rigorously cleaned 25 mm square glass coverslips (600 rpm) for 2 min inside the glovebox. Annealing treatments were carried out under nitrogen on a hot plate at a temperature of 130 °C for up to 300s for both pristine and blend films. Photoluminescence (PL) measurements were carried out on a microscope-based spectrometer equipped with multiple laser excitation sources, electron-multiplying CCD camera and spectrograph (Andor) and long-pass edge filters (Semrock) to reject scattered excitation light that was described in detail previously.[19] Samples were sealed with an aluminum overcoating deposited by high vacuum thermal evaporation techniques, placed in an argon gas flow cell and illuminated in the wide-field configuration. Excitation power densities were ~10 W/cm^2 and no photodegradation effects were observed. PL lifetimes of MDMO-PPV thin films with variable annealing times were measured using a time-correlated single photon counting (TCSPC) module (Becker & Hickl, SPC-130) with pulsed laser excitation and a nominal wavelength of 445 nm (Edinburgh Instruments). PL lifetimes were measured as a function of emission wavelengths by placing narrow bandpass (~10 nm) filters before an avalanche photodiode (APD) detector (id Quantique) that corresponded to the MDMO-PPV PL onset (17 800 cm^{-1}, 560 nm) and tail (13 800 cm^{-1}, 725 nm). Decays were analyzed using a Laplace transform method and the instrument response was determined from measuring scattered light of a blank glass coverslip and found to be ~100 ps. Raman spectra of MDMO-PPV/PCBM thin films of variable PCBM loadings were generated on the same microscope instrument using both short (488 nm) and long (568 nm) excitation wavelengths with the appropriate Rayleigh light rejection filters. Excitation power densities for Raman studies were ~1 kW/cm^2 for both excitation wavelengths and no noticeable photodegradation effects were observed within data acquisition time scales (>10 s). Raman and PL spectra were corrected for instrument response using a tungsten lamp and measured in triplicate to assess sample-to-sample variation effects. Raman spectra were also corrected for self-absorption of scattered light[33] and PL backgrounds were fitted with a polynomial function and subtracted.

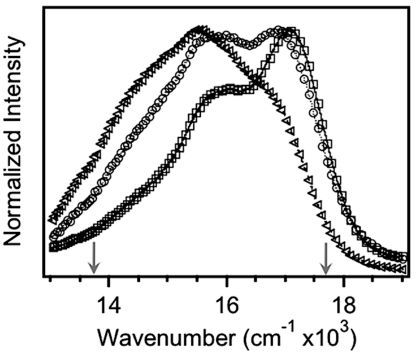

Figure 1. Photoluminescence (PL) spectra of pristine MDMO-PPV thin films with variable annealing times: 0 s, as-cast (□); 30 s (○); 300 s (△). Arrows indicate emission energies used to measure PL lifetimes changes with annealing.

RESULTS

We first examine the conformational and packing characteristics of MDMO-PPV thin films prepared under different conditions (i.e., annealing) in the absence of PCBM with PL spectroscopy. Figure 1 shows PL spectra of MDMO-PPV thin films with variable annealing times (0s, 30s, and 300s at 130 °C). As-cast films show a vibronic line shape pattern similar to that of the solvated polymer (not shown) albeit shifted to lower energy. Upon annealing, several line shape parameters change noticeably: (i) an apparent increase in the Huang−Rhys factor, or suppression of the 0−0 vibronic component intensity, (ii) red shifting of the electronic origin by ~300 cm^{-1}, (iii) line width broadening of vibronic transitions. PL decays for variable annealing MDMO-PPV thin films are shown in Figure 2 measured at two distinct emission wavelengths, namely at the PL onset (blue side, Figure 2a) and tail (red side, Figure 2b) that are indicated by arrows in Figure 1. As-cast (pristine) films and films with short annealing times show nonexponential decays with an instrument-limited component ($\tau_1 \approx 100$ ps) and a longer-lived component ($\tau_2 \approx 350$ ps) for both blue and red tails. Longer annealing times (300s) result in nearly monoexponential decays of $\tau \approx 900$ ps and 1.1 ns measured at both blue and red regions, respectively.

When fullerenes are added to conjugated polymers, the ability of these polymers to close-pack is hindered and PL signatures deviate from the behavior shown in Figures 1 and 2. Figure 3a shows the dependence of the PL 0−0 transition energy (E_{0-0}) for annealed MDMO-PPV and MDMO-PPV/PCBM as-cast films with variable PCBM content are presented in Figure 3b. E_{0-0} values were determined by fitting a Gaussian function to this peak in the PL spectrum (see the Supporting Information) that also reveals the effective range for which the PL transition can be tuned by altering chain conformation and packing. Upon addition of PCBM (Figure 3b), E_{0-0} values show considerable blue-shifts of up to ~600 cm^{-1} and increases of the 0−0 relative intensity that approach values obtained from MDMO-PPV PL spectra in dilute CB solution. These trends suggest that the average conjugation lengths become smaller and chain packing is disabled which is discussed in detail in the following. PCBM loadings higher than ~60% showed large reductions in signal-to-noise ratios

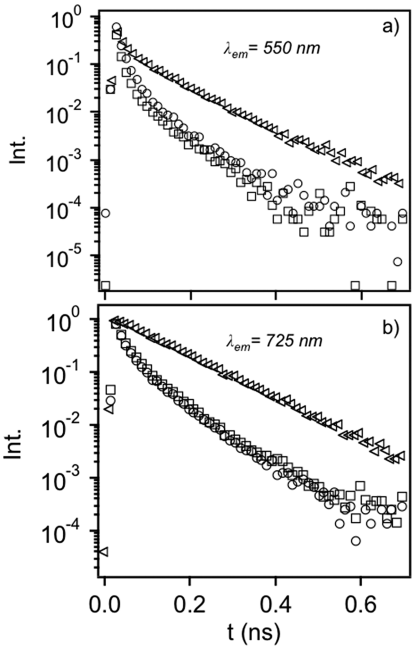

Figure 2. PL lifetimes of pristine MDMO-PPV thin films with variable annealing times: 0s, as-cast (□); 30s (○); 300 s (△) measured at the PL onset (a) and tail (b).

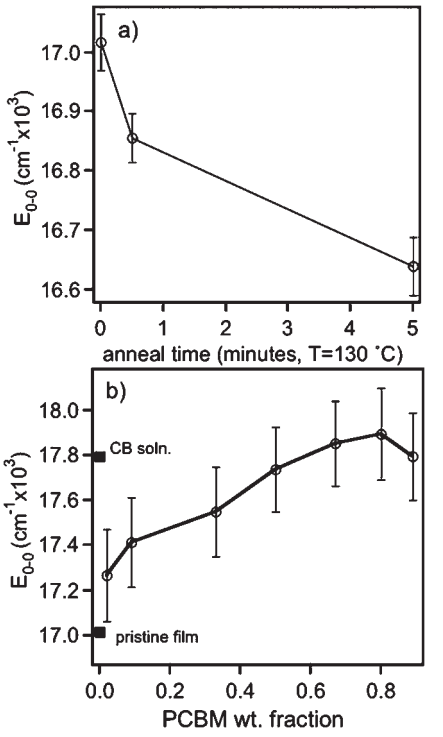

Figure 3. (a) E_{0-0} as a function of annealing time for pristine MDMO-PPV films. (b) Effect of PCBM weight fraction on E_{0-0} of MDMO-PPV PL spectra. E_{0-0} values (■) from chlorobenzene (CB) and pristine thin films are shown for comparison. Error bars correspond to ± one standard deviation of the mean values.

and increased broadening that made the determination of line shape parameters difficult. Fortunately, these limitations can be surpassed by resonance Raman spectroscopy, which provides more reliable information about the changing polymer conformation characteristics with PCBM loading and the specific nature of interaction between the polymer and fullerene molecules.

Figure 4 shows representative Raman spectra for as-cast MDMO-PPV/PCBM thin films with variable PCBM content in the range of 50:1 up to 1:8 w/w with (a) 568 nm and (b) 488 nm excitation wavelengths. These wavelengths were chosen to study the conformational and packing attributes of longer and shorter MDMO-PPV chain segments, respectively, and spectra were recorded in the range of ca. 900—1700 cm^{-1} to monitor changes in MDMO-PPV backbone vibrations. The Raman bands in Figure 4 have been assigned previously for related PPV derivatives[34,35] which correspond to the out-of-plane C−H wag of the vinylene group (~964 cm^{-1}); C−C stretching/C−H bending of the phenyl group (~1111 cm^{-1}); C−C inter-ring stretching (~1280 cm^{-1}); C═C stretching/C−H bending of the vinylene group (~1305 cm^{-1}); C−C stretching of the phenyl group (~1580 cm^{-1}); and C═C stretching of the vinylene group (~1625 cm^{-1}). All Raman spectra were normalized to the dominant ~1580 cm^{-1} mode and changes in intensities and frequencies of Raman bands are determined by fitting each band to a single Lorentzian function. The most noteworthy feature of these spectra is the increase in relative intensities and red-shifts of the vinylene out-of-plane C−H mode (~964 cm^{-1}) with increasing PCBM loading, which are highlighted in the insets of panels a and b in Figure 4. Red-shifts (~4 cm^{-1}) and relative intensity increases were also observed for the MDMO-PPV vinylene C═C symmetric stretch (~1625 cm^{-1}) when blends were excited with 488 nm light. However, 568 nm excitation showed no apparent changes in this band with increasing PCBM loading. Importantly, no frequency

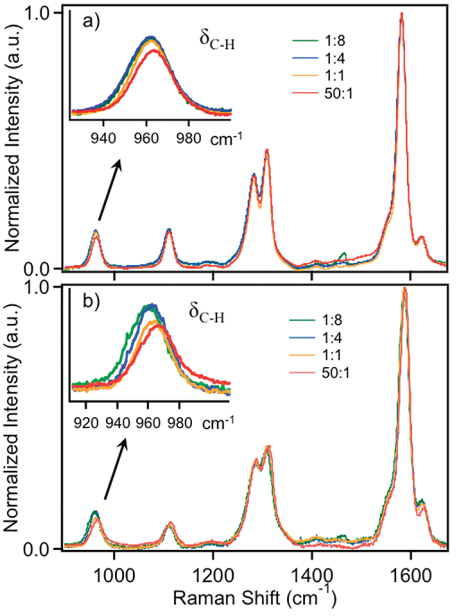

Figure 4. Representative Raman spectra of as-cast MDMO-PPV/PCBM thin films with variable PCBM weight fractions generated with (a) 568 nm and (b) 488 nm excitation wavelengths. Insets show the out-of-plane vinylene C−H wag band of MDMO-PPV (~964 cm^{-1}).

shifts were observed for phenyl group vibrations with the choice of excitation wavelength or PCBM loading implying that refractive index dispersion effects can be ruled out as the origin for the

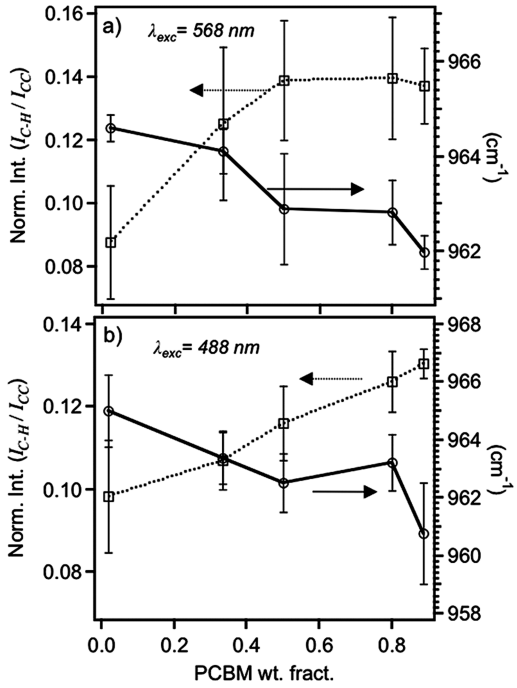

Figure 5. Effect of PCBM weight fraction on the frequency (—○—) and normalized intensity (···□···) of the out-of-plane vinylene C−H wag mode of the MDMO-PPV component for as-cast thin films generated from (a) 568 nm and (b) 488 nm excitation wavelengths. Error bars represent ± one standard deviation of the mean values.

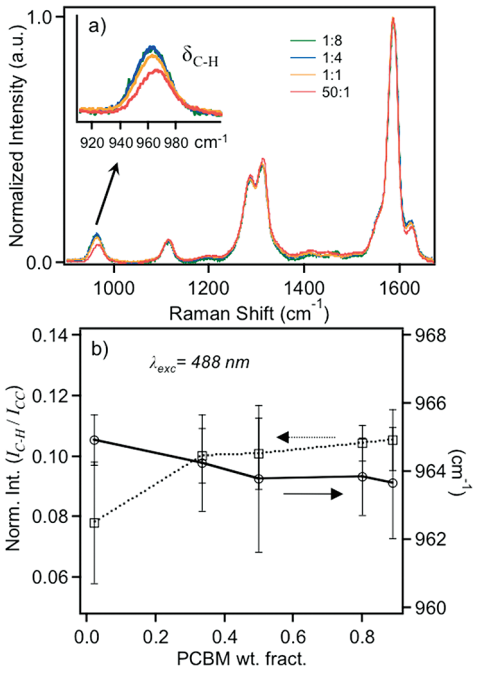

Figure 6. (a) Representative Raman spectra of annealed MDMO-PPV/PCBM thin films with variable PCBM weight fractions generated with 488 nm excitation. The inset shows the ∼964 cm^{-1} band of the out-of-plane C−H wag mode of the vinylene group of MDMO-PPV. (b) Effect of PCBM weight fraction on the frequency (—○—) and intensity (···□···) of the out-of-plane vinylene C−H bending vibration of the MDMO-PPV component. Error bars represent ± one standard deviation of the mean values.

PCBM-dependent shifts of vinylene group modes. Raman transitions from the PCBM component are not observed under the experimental conditions used except at very high loadings (>80%) where the C═C symmetric breathing vibration (∼1460 cm^{-1}) becomes barely discernible in background shot noise. This feature clearly demonstrates the high sensitivity and selectivity of resonance Raman spectroscopy to interrogate polymer structure in blends with large acceptor loadings that is not possible using PL spectroscopy. To further understand the nature of MDMO-PPV structural distortions with varying PCBM content we turn our attention to the ∼964 cm^{-1} mode to establish how MDMO-PPV/PCBM interactions influence polymer conformations.

Figure 5 shows the effect of PCBM content on the relative intensities and frequencies of the MDMO-PPV ∼964 cm^{-1} mode. Both excitation wavelengths show similar trends with the same PCBM loading but spectra excited with 568 nm light show less pronounced red shifts (∼3 cm^{-1}) compared to red shifts of up to 5 cm^{-1} for spectra excited with 488 nm light. The relative intensities of this mode (I_{C-H}/I_{CC}) show increases of up to ∼30% between the lowest (50:1 w/w) and highest (1:8 w/w) PCBM loading for both excitation wavelengths. The overall similarity of the relative intensity increases and red-shifts of the ∼964 cm^{-1} mode for short and long wavelength excitation suggest that PCBM interactions for both short and long chain segments are likewise similar. We consider the origins for these changes in detail in the Discussion section.

Annealing treatments (130 °C, 5 min) were applied to MDMO-PPV/PCBM films to promote phase separation between both components and Raman spectra for various PCBM loadings are shown in Figure 6. Figure 6a shows Raman spectra for annealed MDMO-PPV/PCBM films excited at 488 nm and Figure 6b shows intensity and frequency changes with varying PCBM content. Importantly, the relative intensities of the ∼964 cm^{-1} mode were considerably smaller in annealed films compared to as-cast films of the same PCBM loading and showed increases of only ∼15% over the entire range of PCBM loadings studied. Frequency shifts of this mode are also diminished compared to as-cast films which only red-shift by ∼2 cm^{-1} between loadings of 50:1 to 1:8 w/w. Furthermore, linewidths of the ∼964 cm^{-1} mode were slightly narrower indicating less overall disorder in the annealed films. On the other hand, red-shifts of up to 3 cm^{-1} were observed in the ∼1625 cm^{-1} mode in annealed films which are comparable to the red-shifts found in as-cast films using 488 nm excitation. Raman spectra of annealed films with large PCBM loadings using 568 nm excitation showed larger PL backgrounds and low signal-to-noise ratios. We have therefore excluded these data from further comparison and analysis.

DISCUSSION

Polymer spectroscopic lineshapes and photophysics have long been known to be sensitive to chain conformations and interactions. Spectroscopic manifestations of chain−chain interactions are diminished PL yields and 0−0 intensities in addition to prominent red-shifts, as a result of a greater number of $\pi-\pi$ stacked chains at the bottom of excited state energy funnels. Intuitively, these interactions should be most favorable when individual polymer chain conformations are elongated and coplanarity exists between individual segments. Aggregation occurs either by the polymer chain folding back onto itself

(intrachain) or through interactions between neighboring polymer chains (interchain) but these structures can be difficult to distinguish solely from PL spectroscopy. Previous IR and Raman spectroscopic studies of unsubstituted PPV derivatives showed that chains tend to planarize and close-pack as seen from significant decreases of the intensities of the out-of-plane C−H wag of the vinylene group (~963 cm^{-1}) but this effect may diminish when solubilizing side groups are present.[34] Because of the relatively low molecular weight of the MDMO-PPV sample used in this study, interchain aggregation is expected to dominate upon annealing. Excitation energy funneling to low-energy interchain sites should likewise be enhanced and PL lineshapes can then be used to assess the nature of interchain coupling. Increased interchain interactions and coupling are readily apparent from the PL trends in Figure 1 where annealing causes ~300 cm^{-1} red-shift of PL energies, line width broadening and apparent increase of the line shape Huang−Rhys factors with longer annealing times.[23,24]

Application of hydrostatic pressures on conjugated polymers is also known to modify interchain interactions and coupling and pressure-dependent PL spectra can be used to assess changes in chain conformation and packing. For example, PL spectra of related PPV derivatives under pressure exhibit significant reductions in the 0−0 transition intensity as well as overall red-shifts and broader linewidths that are similar to the observed changes in PL spectra of annealed films (Figure 1).[36−38] The structural origins of these pressure-dependent changes are believed to be a planarization of the conjugated backbone that enables better interchain electronic communication.[39,40] These structural deformations and subsequent improvements in interchain interactions can promote the formation of H-aggregates that bear resemblance to the PL line shape changes shown in Figure 1 (i.e., non-Poissonian line shape profiles). Because polymer chain disorder causes deviations from ideal H-aggregate lineshapes, the weakly coupled H-aggregate model developed by Spano and coworkers is frequently used for describing the strength of interchain coupling in polymer systems as well as its dependence on competing intra- and interchain order.[29] Although the annealing-dependent changes in PL lineshapes shown in Figure 1 are consistent with predictions from the weakly coupled H-aggregate model when interchain coupling increases, the strong red-shifts and broadening effects observed in MDMO-PPV PL spectra with longer annealing times suggests that interchain electronic coupling in this system does not fall within the weakly coupled regime. In this case, excited-state interactions begin to dominate and PL spectra resemble excimer-like transitions. To better understand the extent of interchain coupling and their implications on PL signatures, we turn to PL lifetime data, which helps sort out ambiguities of PL lineshapes.

Comparison of PL decays measured at either the blue onset or red tail of the PL line shape reveal similar characteristics albeit a ~20% larger contribution of the fast (instrument limited) component observed for decays measured on the PL onset (~550 nm). Because polymer chains cast from solution primarily exist in distorted conformations, interchain packing is not optimal and represents the smaller contribution to the decay profile. PL decays for pristine (as-cast) and films annealed for short times (~30 s) more closely resemble those of dilute solutions that are typically nonexponential indicating incomplete energy funneling. The short- and longer-lived components of these decays likely correspond to emission from partially aggregated chains and distorted chains, respectively. Annealing films for longer times results in better interchain interactions and stronger electronic coupling between neighboring segments. Correspondingly, lifetimes were nearly single exponential, demonstrating complete energy funneling to interchain sites. The long decay times and broad, red-shifted spectra for MDMO-PPV films annealed >300s resemble excimer-like transitions that have been observed in other PPV derivatives.[41,42] These data suggest a two-emitter system comprised of both intra- and interchain species, the latter exhibiting a wide range of electronic coupling strength depending on the conformational attributes of the chains. Assuming exciton migration lengths of ~4−5 nm, as little as one of these sites within this range can dominate the PL spectral and decay features. Schwartz and co-workers observed similar trends in MEH-PPV films that were also attributed to increased interchain interactions. Based on the changes in vibronic line shape and decay features in Figures 1−3a, we conclude that MDMO-PPV chains planarize upon annealing that results in a larger number of interchain contacts. We now use these trends in PL signatures as a basis for understanding changes in polymer conformations and packing upon addition of PCBM as well as the specific nature of interactions between polymer and fullerene molecules in blends.

When PCBM is added to MDMO-PPV, PL spectra show blue-shifts of the 0−0 transitions and apparent reductions in the line shape Huang−Rhys factors (Figure 3b). These results suggest that PCBM disables interchain interactions leading to more disordered chain conformations with shorter conjugation lengths. In addition to shifting PL energies, the vibronic intervals provide important insights into changes in chain conformation and packing that change depending on the sample processing conditions and addition of acceptor molecules. For example, we previously described the appearance of the missing mode effect (MIME) in MDMO-PPV PL spectra where the observed vibronic interval represents the coalescence of transitions from the backbone modes presented in Figure 4.[31] The contributions (displacements) of each Franck−Condon active mode were found to be sensitive to material processing conditions that caused the observed MIME intervals to increase by up to ~150 cm^{-1} between dilute solutions and annealed films. Interestingly, corresponding Raman studies showed that the ~964 cm^{-1} out-of-plane C−H wag was the most sensitive to changes in the polymer structure, namely, increased intrachain order and interchain packing. Although addition of PCBM caused further decreases in the contribution of the ~964 cm^{-1} mode, it was not possible to accurately quantify polymer structural changes with larger PCBM concentrations due to increased quenching and line shape broadening. These fundamental limitations of PL spectroscopy to track changes in polymer structure and interactions with large acceptor loadings necessitate the use of Raman spectroscopy that is capable of uncovering changes in the polymer structure over a wider range of PCBM loadings.

Comparison of Raman spectra excited with short and long excitation wavelengths reveal important changes in MDMO-PPV structure upon addition of PCBM. As shown in Figures 4 and 5, the red-shifts and increasing relative intensities of the MDMO-PPV ~964 cm^{-1} mode show that PCBM molecules interact preferentially with this backbone group which is also apparent from the invariance of other (phenyl) backbone modes to changing PCBM content. Previously, Bruevich et al. showed that addition of trinitrofluorenone (TNF) to structurally similar MEH-PPV chains cause marked decreases of the out-of-plane

vinylene C−H wag intensities along with blue-shifts of up to 7 cm^{-1}. These changes were also accompanied by red-shifted and broadened absorption transitions due to ground-state charge transfer interactions between MEH-PPV and TNF molecules.[20,21] Because of the forbidden nature of the out-of-plane C−H wag mode when polymer segments are planarized, these authors concluded that MEH-PPV and TNF molecules interact in a cofacial manner resulting in an increase of planarity of MEH-PPV segments. In contrast, the red-shifts and increasing intensities of the ∼964 cm^{-1} mode in MDMO-PPV/PCBM blends (Figures 4 and 5) demonstrate that larger PCBM concentrations cause a decrease in planarity between chain segments. These distortions should likewise result in shorter conjugation lengths, blue-shifts and spectral broadening of PL spectra with increasing PCBM loading. The PL trends in Figure 3b are in fact consistent with this observation. Based on these trends and previous analyses of the MDMO-PPV PL MIME intervals, polymer chain conformations become more solution-like (disordered) with larger amounts of PCBM. Another, but less likely, explanation for the changes in the ∼964 cm^{-1} mode is a distortion from a trans to cis arrangement of the PPV backbone which would lower the effective idealized symmetry ($\sim C_{2h}$) and make this mode allowed in the new point group ($\sim C_{2v}$). However, this situation would result in drastically different Raman spectra because of more modes becoming allowed in the lower point group, which is not observed. We now consider the specific nature of interaction between MDMO-PPV and PCBM molecules in the blend films and its role on the observed structural deformations of MDMO-PPV chains.

McGehee and co-workers recently proposed that intercalation of acceptor molecules (i.e., PCBM) into MDMO-PPV alkoxy side groups causes a conformation change of the polymer that lead to improved charge transport characteristics relative to pristine films. In particular, acceptor intercalation was believed to cause an elongation of the polymer conformation, increased intrachain order (planarity) and more interchain interactions. Although no direct evidence for these conformational and packing changes was provided, electron micrographs of blends showed relatively uniform features indicating that the MDMO-PPV and acceptor molecules existed in a mixed phase.[11] Moreover, PL quenching in fullerene blends was nearly quantitative which further supports intercalation but does not provide insights into changes of the MDMO-PPV conformation and packing. We propose that the sensitivity of the out-of-plane C−H wag and C═C symmetric stretching vibrations of MDMO-PPV vinylene group to PCBM loading results from intercalation of these acceptors into the polymer side groups. The preferential nature of this interaction is surprising and has important implications for understanding the mechanisms of both charge generation and transport in MDMO-PPV/PCBM blends. This hypothesis was tested further by applying annealing treatments to MDMO-PPV/PCBM blends and measuring Raman spectra (Figure 6). Because annealing promotes phase separation between polymer and fullerene components, we expect that removal of intercalated PCBM molecules from polymer side groups should partially restore intrachain order and interchain packing. In this scheme, frequency and intensity changes in the ∼964 cm^{-1} should be suppressed in annealed films compared to those measured from as-cast films for similar loadings. Figure 6 indeed shows that both red-shifts and intensity increases for the ∼964 cm^{-1} mode are substantially smaller than those observed in as-cast films excited with either 488 or 568 nm light. Because of the relatively short annealing times used here (∼5 min vs 1 h in ref 11) there is still a significant amount of a mixed phase that gives rise to the nonzero shifts of the ∼964 cm^{-1} mode shown in Figure 6. Nonetheless, the PL and Raman data presented herein as well as results from previous structural studies provide strong evidence of not only intercalation of fullerene acceptors but also the preferential nature of interaction between these molecules and polymer chain segments.

The structural distortions incurred in the MDMO-PPV component can now be used to better understand and refine the previously proposed structural mechanisms of enhanced charge mobility in PCBM blends. First, PL and Raman data convincingly demonstrate that polymer chains become more distorted with addition of PCBM with the dominant distortion being the loss of coplanarity between chain segments that causes a decrease of conjugation lengths and interchain interactions. This result demonstrates that the previously proposed increase in intrachain order (planarization of chain segments) does not occur in MDMO-PPV/PCBM blends. Gelinck et al. also demonstrated that decreased conjugation lengths and intrachain order resulted in lower charge photoconductivities when polymers were subject to photo-oxidation,[43] which would likewise suggest similar decreases in charge mobilities in MDMO-PPV/PCBM blends. Because interchain interactions are affected by intrachain order, it is now important to consider how these structural interactions impact charge transport in MDMO-PPV/PCBM blends.

Annealing of MDMO-PPV/PCBM blend films was shown to cause reductions of charge mobilities to levels similar to those observed in pristine MDMO-PPV films.[11] However, Raman spectra of annealed MDMO-PPV/PCBM films confirmed that interchain interactions are partially restored (as seen from diminished red-shifts and intensity increases of the ∼964 cm^{-1} mode) when intercalated fullerenes begin to phase separate allowing neighboring polymer chain segments to interact. This effect was also demonstrated for pristine and lightly doped films where significant intensity decreases and blue-shifts of the ∼964 cm^{-1} occurred with annealing,[31] opposite to the trends shown in as-cast films (Figures 4 and 5) where interchain interactions are suppressed. These results imply that interchain interactions also cannot be considered as a structural origin for mobility enhancements when acceptors intercalate into the polymer structure.

Lastly, the overall chain conformation can have a significant impact on charge mobilities. For example, charge mobilities can vary greatly depending on whether the chains adopt collapsed or elongated conformations. It was previously suggested that intercalation of acceptors causes an elongation of the polymer chains that, together with the proposed increase in intra- and interchain order, lead to better charge mobilities. We speculate, based on trends from PL data of pristine MDMO-PPV films and Raman spectra of MDMO-PPV/PCBM films, that polymer chains are likely in elongated conformations. However, our present data do not allow us to definitively confirm this assignment and further work is needed to determine the specific chain conformations in blends.

After ruling out chain planarization and increasing interchain interactions as the origins for improved charge mobilities, we now consider changes in electronic interactions between polymer and fullerene components. For example, ground-state

charge transfer interactions could result in improved charge mobilities because of the intimately mixed nature of both components. On the other hand, intercalation of PCBM may modify Franck−Condon factors for charge transfer along the polymer backbone possible causing reductions of reorganization energies. Because our data do not allow us to directly assess changes in charge transfer reorganization energies, we instead focus on the possibility of ground state charge transfer interactions as a source of improved mobilities.

Ground-state charge transfer interactions typically appear as weak, broadened and red-shifted optical transitions and the structural attributes of these states can be investigated by resonance Raman spectroscopy. Bruevich et al. used this approach to study charge transfer interactions in MEH-PPV/TNF blends that resulted in new absorption features as well as red-shifts of up to ∼5 cm^{-1} of the dominant ∼1580 cm^{-1} C−C stretching mode of the MEH-PPV phenyl group with increasing TNF concentration. These charge transfer interactions were found to be favorable when MEH-PPV segments and TNF acceptors pack in a cofacial manner thus promoting the planarization of MEH-PPV segments. In contrast, optical absorption spectra of MDMO-PPV/PCBM blend films showed no new apparent transitions near the onset region and spectra could be reproduced as a linear superposition of each component (see the Supporting Information). However, it is conceivable that these transitions may be masked by more strongly allowed $\pi-\pi^*$ transitions because of their low oscillator strengths and not readily observable using linear spectroscopic techniques. This was in fact confirmed by recent photomodulation and electroluminescence spectroscopic studies of various PPV/fullerene blends that demonstrate significant charge transfer character exists in these systems.[44,45] We speculate that the preferential interaction between PCBM molecules and the vinylene group of MDMO-PPV may help understand the orbital parentage of these states and their dependence on polymer structure and blend morphology. If increased charge transfer character is present in MDMO-PPV/PCBM blends, these effects should be discernible from spectral shifts of key backbone modes by comparing Raman spectra excited with different wavelengths.

It was previously shown in Figures 4b and 6a that the MDMO-PPV C═C vinylene stretching band (∼1625 cm^{-1}) intensity increases and red-shifts with increasing PCBM content. These red-shifts are reminiscent to those observed for the ∼1580 cm^{-1} mode of MEH-PPV/TNF blends due to ground-state charge transfer. Because the C═C stretching modes of both backbone groups are sensitive to changes in the π electronic structure of the polymer component, it is possible that the observed red-shifts of the ∼1625 cm^{-1} reflect ground state charge transfer complex formation. However, these changes were observed only for spectra generated with 488 nm light, which is unexpected for ground-state charge transfer interactions since these transitions usually fall below the absorption onset (band edge). A more plausible explanation for the changes in the ∼1625 cm^{-1} mode could simply be decreasing conjugation lengths and localization of charge density along the backbone, which is supported by the observed blue-shifts of PL E_{0-0} values with PCBM content (Figure 3b). In addition, we would expect concomitant frequency shifts in the dominant ∼1580 cm^{-1} mode of the MDMO-PPV phenyl group, which are not observed. To rule out charge transfer resonance or conjugation length changes, we are presently pursuing studies of resonance Raman excitation profiles that should be able to distinguish either mechanism.

CONCLUSIONS

The PL and Raman results presented here have shown that intercalation of PCBM into MDMO-PPV side groups causes a decrease in intrachain order and conjugation lengths. Furthermore, these distortions inhibit interchain interactions but can be restored upon annealing. The nature of these structural changes effectively rule out previously proposed increases in MDMO-PPV chain planarization and interchain interactions as the origins of improved charge mobilities in fullerene blends. Our PL and Raman data do not allow us to conclude whether chain elongation occurs but this appears to be consistent with chain conformations becoming more solution-like with larger PCBM loadings. On the other hand, we suspect that ground-state charge transfer interactions and possibly lower reorganization energies due to intercalation of PCBM could be playing significant roles in both charge generation and transport in MDMO-PPV/PCBM blends. These topics are the subject of further investigations by our group.

ASSOCIATED CONTENT

Supporting Information. PL and absorption spectra of MDMO-PPV/PCBM blends. This material is available free of charge via the Internet at http://pubs.acs.org.

AUTHOR INFORMATION

Corresponding Author
*E-mail: jkgrey@unm.edu.

ACKNOWLEDGMENT

J.K.G. acknowledges support from the National Science Foundation (CHE-0955242) and A.J.W. acknowledges support from a GAANN fellowship from the U.S. Department of Education.

REFERENCES

(1) Schwartz, B. J. *Annu. Rev. Phys. Chem.* **2003**, *54*, 141–172.
(2) Sims, M.; Tuladhar, S. M.; Nelson, J.; Maher, R. C.; Campoy-Quiles, M.; Choulis, S. A.; Mairy, M.; Bradley, D. D. C.; Etchegoin, P. G.; Tregidgo, C.; Suhling, K.; Richards, D. R.; Massiot, P.; Nielsen, C. B.; Steinke, J. H. G. *Phys. Rev. B* **2007**, *76*, 195206/1–195206/12.
(3) Hallermann, M.; Kriegel, I.; Da Como, E.; Berger, J. M.; von Hauff, E.; Feldmann, J. *Adv. Funct. Mater.* **2009**, *19*, 3662–3668.
(4) Gao, Y.; Martin, T. P.; Niles, E. T.; Wise, A. J.; Thomas, A. K.; Grey, J. K. *J. Phys. Chem. C* **2010**, *114*, 15121–15128.
(5) Mayer, A. C.; Toney, M. F.; Scully, S. R.; Rivnay, J.; Brabec, C. J.; Scharber, M.; Koppe, M.; Heeney, M.; McCulloch, I.; McGehee, M. D. *Adv. Funct. Mater.* **2009**, *19*, 1173–1179.
(6) Cates, N. C.; Gysel, R.; Beiley, Z.; Miller, C. E.; Toney, M. F.; Heeney, M.; McCulloch, I.; McGehee, M. D. *Nano Lett.* **2009**, *9*, 4153–4157.
(7) Tremblay, N. J.; Gorodetsky, A. A.; Cox, M. P.; Schiros, T.; Kim, B.; Steiner, R.; Bullard, Z.; Sattler, A.; So, W.-Y.; Itoh, Y.; Toney, M. F.; Ogasawara, H.; Ramirez, A. P.; Kymissis, I.; Steigerwald, M. L.; Nuckolls, C. *ChemPhysChem* **2010**, *11*, 799–803.
(8) Szarko, J. M.; Guo, J.-C.; Liang, Y.-Y.; Lee, B.-D.; Rolczynski, B. S.; Strzalka, J.; Xu, T.; Loser, S.; Marks, T. J.; Yu, L.-P.; Chen, L.-X. *Adv. Mater.* **2010**, *22*, 5468–5472.

(9) Chen, D.; Nakahara, A.; Wei, D.; Nordlund, D.; Russell, T. P. *Nano Lett.* **2011**, *11*, 561–567.
(10) Collins, B. A.; Gann, E.; Guignard, L.; He, X.; McNeill, C. R.; Ade, H. *J. Phys. Chem. Lett.* **2010**, *1*, 3160–3166.
(11) Cates, N. C.; Gysel, R.; Dahl, J. E. P.; Sellinger, A.; McGehee, M. D. *Chem. Mater.* **2010**, *22*, 3543–3548.
(12) Melzer, C.; Koop, E. J.; Mihailetchi, V. D.; Blom, P. W. M. *Adv. Funct. Mater.* **2004**, *14*, 865–870.
(13) Tuladhar, S. M.; Poplavskyy, D.; Choulis, S. A.; Durrant, J. R.; Bradley, D. D. C.; Nelson, J. *Adv. Funct. Mater.* **2005**, *15*, 1171–1182.
(14) Myers, A. B. *Adv. Multi-Photon Proc. Spec.* **1998**, *11*, 3–50.
(15) Heimel, G.; Somitsch, D.; Knoll, P.; Bredas, J.-L.; Zojer, E. *J. Chem. Phys.* **2005**, *122*, 114511/1–114511/9.
(16) Furukawa, Y.; Sakamoto, A.; Ohta, H.; Tasumi, M. *Synth. Met.* **1992**, *49*, 335–40.
(17) Furukawa, Y. *J. Phys. Chem.* **1996**, *100*, 15644–15653.
(18) Tuladhar, S. M.; Sims, M.; Kirkpatrick, J.; Maher, R. C.; Chatten, A. J.; Bradley, D. D. C.; Nelson, J.; Etchegoin, P. G.; Nielsen, C. B.; Massiot, P.; George, W. N.; Steinke, J. H. G. *Phys. Rev. B* **2009**, *79*, 035201/1–035201/10.
(19) Gao, Y.; Grey, J. K. *J. Am. Chem. Soc.* **2009**, *131*, 9654–9662.
(20) Bruevich, V. V.; Makhmutov, T. S.; Elizarov, S. G.; Nechvolodova, E. M.; Paraschuk, D. Y. *J. Chem. Phys.* **2007**, *127*, 104905/1–104905/9.
(21) Bruevich, V. V.; Makhmutov, T. S.; Elizarov, S. G.; Nechvolodova, E. M.; Paraschuk, D. Y. *J. Exp. Theor. Phys.* **2007**, *105*, 469–478.
(22) Yan, M.; Rothberg, L. J.; Kwock, E. W.; Miller, T. M. *Phys. Rev. Lett.* **1995**, *75*, 1992–5.
(23) Nguyen, T.-Q.; Doan, V.; Schwartz, B. J. *J. Chem. Phys.* **1999**, *110*, 4068–4078.
(24) Nguyen, T.-Q.; Martini, I. B.; Liu, J.; Schwartz, B. J. *J. Phys. Chem. B* **2000**, *104*, 237–255.
(25) Collison, C. J.; Rothberg, L. J.; Treemaneekarn, V.; Li, Y. *Macromolecules* **2001**, *34*, 2346–2352.
(26) Kemerink, M.; van Duren, J. K. J.; Jonkheijm, P.; Pasveer, W. F.; Koenraad, P. M.; Janssen, R. A. J.; Salemink, H. W. M.; Wolter, J. H. *Nano Lett.* **2003**, *3*, 1191–1196.
(27) Kemerink, M.; van Duren, J. K. J.; van Breemen, A. J. J. M.; Wildeman, J.; Wienk, M. M.; Blom, P. W. M.; Schoo, H. F. M.; Janssen, R. A. J. *Macromolecules* **2005**, *38*, 7784–7792.
(28) Bittner, E. R.; Karabunarliev, S.; Herz, L. M. *J. Chem. Phys.* **2007**, *126*, 191102/1–191102/4.
(29) Spano, F. C. *Acc. Chem. Res.* **2010**, *43*, 429–439.
(30) Yang, G.; Li, Y.; White, J. O.; Drickamer, H. G. *J. Phys. Chem. B* **1999**, *103*, 5181–5186.
(31) Wise, A. J.; Martin, T. P.; Gao, J.; Van Der Geest, K.; Grey, J. K. *J. Chem. Phys.* **2010**, *133*, 174901–174910.
(32) Tutt, L.; Tannor, D.; Schindler, J.; Heller, E. J.; Zink, J. I. *J. Phys. Chem.* **1983**, *87*, 3017–19.
(33) Shriver, D. F.; Dunn, J. B. R. *Appl. Spectrosc.* **1974**, *28*, 319–23.
(34) Sakamoto, A.; Furukawa, Y.; Tasumi, M. *J. Phys. Chem.* **1992**, *96*, 1490–4.
(35) da Silva, M. A. T.; Dias, I. F. L.; Duarte, J. L.; Laureto, E.; Silvestre, I.; Cury, L. A.; Guimaraes, P. S. S. *J. Chem. Phys.* **2008**, *128*, 094902/1–094902/7.
(36) Tikhoplav, R. K.; Hess, B. C. *Synth. Met.* **1999**, *101*, 236–237.
(37) Zeng, Q. G.; Ding, Z. J.; Ju, X.; Zhang, Z. M. *Eur. Polym. J.* **2005**, *41*, 743–746.
(38) Paudel, K.; Arif, M.; Chandrasekhar, M.; Guha, S. *Phys. Status Solidi B* **2009**, *246*, 563–569.
(39) Guha, S.; Graupner, W.; Resel, R.; Chandrasekhar, M.; Chandrasekhar, H. R.; Glaser, R.; Leising, G. *Synth. Met.* **1999**, *101*, 180–181.
(40) Guha, S.; Graupner, W.; Resel, R.; Chandrasekhar, M.; Chandrasekhar, H. R.; Glaser, R.; Leising, G. *J. Phys. Chem. A* **2001**, *105*, 6203–6211.
(41) Jakubiak, R.; Collison, C. J.; Wan, W. C.; Rothberg, L. J.; Hsieh, B. R. *J. Phys. Chem. A* **1999**, *103*, 2394–2398.
(42) Chen, S. H.; Su, A. C.; Han, S. R.; Chen, S. A.; Lee, Y. Z. *Macromolecules* **2004**, *37*, 181–186.
(43) Gelinck, G. H.; Warman, J. M. *Chem. Phys. Lett.* **1997**, *277*, 361–366.
(44) Vandewal, K.; Gadisa, A.; Oosterbaan, W. D.; Bertho, S.; Banishoeib, F.; Van Severen, I.; Lutsen, L.; Cleij, T. J.; Vanderzande, D.; Manca, J. V. *Adv. Funct. Mater.* **2008**, *18*, 2064–2070.
(45) Drori, T.; Sheng, C. X.; Ndobe, A.; Singh, S.; Holt, J.; Vardeny, Z. V. *Phys. Rev. Lett.* **2008**, *101*, 037401/1–037401/4.